Cell

Biogenesis of a Bacterial Organelle: The Carboxysome Assembly Pathway

Jeffrey C. Cameron,[1] Steven C. Wilson,[1] Susan L. Bernstein,[2] and Cheryl A. Kerfeld[1,2,3,*]
[1]Department of Plant and Microbial Biology, University of California, Berkeley, Berkeley, CA 94720, USA
[2]U.S. Department of Energy-Joint Genome Institute, Walnut Creek, CA 94598, USA
[3]Synthetic Biology Institute, University of California, Berkeley, Berkeley, CA 94720, USA
*Correspondence: ckerfeld@lbl.gov
http://dx.doi.org/10.1016/j.cell.2013.10.044

SUMMARY

The carboxysome is a protein-based organelle for carbon fixation in cyanobacteria, keystone organisms in the global carbon cycle. It is composed of thousands of subunits including hexameric and pentameric proteins that form a shell to encapsulate the enzymes ribulose 1,5-bisphosphate carboxylase/oxygenase and carbonic anhydrase. Here, we describe the stages of carboxysome assembly and the requisite gene products necessary for progression through each. Our results demonstrate that, unlike membrane-bound organelles of eukaryotes, in carboxysomes the interior of the compartment forms first, at a distinct site within the cell. Subsequently, shell proteins encapsulate this procarboxysome, inducing budding and distribution of functional organelles within the cell. We propose that the principles of carboxysome assembly that we have uncovered extend to diverse bacterial microcompartments.

INTRODUCTION

In contrast to the membrane-bound organelles of eukaryotes, many bacteria sequester diverse metabolic pathways in protein-based organelles, bacterial microcompartments (BMCs) (Bobik, 2006; Cannon et al., 2001; Cheng et al., 2008; Kerfeld et al., 2010; Yeates et al., 2008). BMCs structurally resemble icosahedral viral capsids; hexameric and pentameric protein subunits comprise a shell that encapsulates densely packed enzyme particles. This compartmentalization of reactions provides a means to increase substrate concentration thereby improving the catalytic efficiency of encapsulated enzymes. The shell also provides a barrier to prevent potentially toxic intermediates from diffusing into the cytoplasm. While bacterial microcompartments were long thought to be a rarity, glimpsed only occasionally in electron micrographs, it is now clear that many bacteria contain BMCs. In fact, the presence of BMC shell homologs in bacterial species across 13 phyla suggests that metabolic compartmentalization is a common feature among diverse prokaryotes (Kerfeld et al., 2010).

Three types of BMCs that have been extensively characterized are involved in the metabolism of 1,2-propanediol (Pdu metabolosome) (Bobik et al., 1999; Parsons et al., 2008), ethanolamine (Eut metabolosome) (Brinsmade et al., 2005; Kofoid et al., 1999; Stojiljkovic et al., 1995), and in CO_2 fixation (carboxysome) (Cannon et al., 1991; Price and Badger, 1991; Shively et al., 1973); common features of the encapsulated pathways are the presence of a reactive or volatile intermediate or an oxygen sensitive enzyme (Kerfeld et al., 2010; Yeates et al., 2008).

The carboxysome is a BMC that plays a central role in the Calvin-Benson-Bassham cycle in cyanobacteria and some chemoautotrophs (Figure 1A) (Price et al., 1992; Shively et al., 1973); it contributes to a major fraction of the Earth's primary productivity by participating in carbon fixation in marine, freshwater, and terrestrial ecosystems. The carboxysome is the core component of the cyanobacterial carbon concentrating mechanism. In the carboxysome the concentration of CO_2 is increased in proximity to the carbon fixing enzyme ribulose 1, 5-bisphosphate carboxylase/oxygenase (RuBisCO) thereby reducing its reaction with O_2, a competing substrate (Cannon et al., 2001; Marcus et al., 1992; Price et al., 2008).

The majority of the morphologically and ecophysiologically diverse cyanobacteria, including the model organism *Synechococcus elongatus* PCC 7942 (*Synechococcus* PCC7942), contain β-carboxysomes that encapsulate plant-like, Form 1B RuBisCO. Because carbon fixation is essential for photoautotrophic growth, *Synechococcus* PCC7942 positions carboxysomes along the longitudinal axis of the cell to ensure distribution of the organelle to each daughter cell (Savage et al., 2010). Formation of additional functional carboxysomes de novo requires the coordinated assembly of thousands of individual protein subunits, ultimately leading to the encapsulation of hundreds of copies of the enzymes RuBisCO and carbonic anhydrase within a protein shell. However, how this intricate self-assembly process is accomplished is unknown.

Many of the structural and catalytic components of the carboxysome have been identified through genetic screens (Price and Badger, 1989; Price and Badger, 1991), including the *ccm* operon that encodes the shell proteins (CcmK2, CcmL, and CcmO) and two other proteins, CcmM and CcmN, thought to participate in the organization of the carboxysome interior (Kinney et al., 2012; Long et al., 2007) (Figure 1B). In *Synechococcus* PCC7942, the genes encoding RuBisCO (*rbcL* and *rbcS*) are

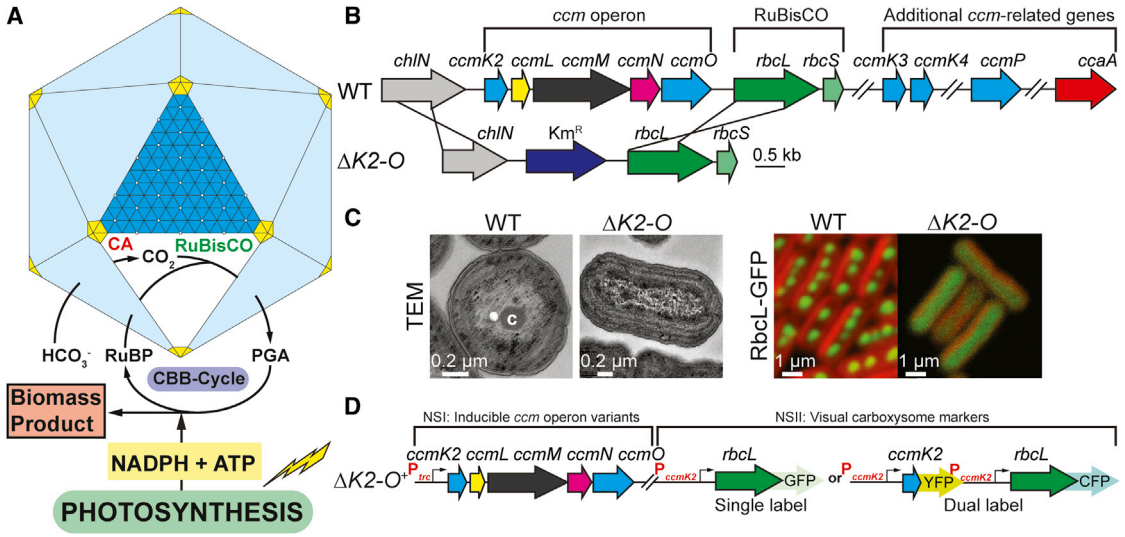

Figure 1. A System to Investigate Carboxysome Biogenesis

(A) The carboxysome shell is comprised of hexameric (blue) and pentameric (yellow) proteins that encapsulate key enzymes of the Calvin-Benson-Bassham cycle (CBB-Cycle) essential for carbon fixation.

(B) Structural (CcmM, black; CcmN, magenta) and catalytic components (RubisCO, green; CcaA, red) of the β-carboxysome are located in the *ccm* operon and elsewhere in the chromosome of *Synechococcus elongatus* PCC 7942. The Δ*K2-O* strain was generated by deletion of the *ccm* operon.

(C) Microscopic characterization of WT and Δ*K2-O* strains showing presence (WT) and absence (Δ*K2-O*) of carboxysomes (labeled with C).

(D) An inducible version of the *ccm* operon was introduced into the Δ*K2-O* mutant to generate the Δ*K2-O*$^{+}$ strain.

See Figure S1 for additional experimental details.

located adjacent to the *ccm* operon, while genes encoding additional carboxysome components (*ccmK3*, *ccmK4*, *ccmP*, and *ccaA*) reside in distant loci and are not essential for carboxysome formation (Rae et al., 2012; So et al., 2002). X-ray crystallographic studies have revealed detailed structures of shell proteins (Kerfeld et al., 2005; Tanaka et al., 2008), providing the foundation for an atomic level model of a carboxysome resembling an icosahedron.

Genetic deletion analysis has led to the identification of the protein components that are essential for carboxysome formation including CcmK, CcmM, and CcmN; knockouts of each result in strains lacking carboxysomes. Recent biochemical studies have shed some light on peptide sequences involved in facilitating interactions between the shell and the interior of the carboxysome and of other BMCs (Fan et al., 2012; Kinney et al., 2012). In the cyanobacterium *Synechococcus* PCC7942, one such peptide, on the C terminus of CcmN, is critical for carboxysome formation (Kinney et al., 2012). Furthermore, domains resembling the small subunit of RuBisCO (RbcS-like domains) on the C terminus of CcmM are also required components of the carboxysome (Long et al., 2010). While these studies identify the essential structural components carboxysomes, they do not provide information on the hierarchy of protein-protein interactions that organize the carboxysome as it forms. Investigation of the assembly of carboxysomes has relied on static images provided by electron microscopy (Iancu et al., 2010; Orus et al., 1995; Price and Badger, 1991); the inherent difficulty in unambiguously identifying assembly intermediates in these studies has left a major gap in our understanding of the dynamics of the assembly process.

In this work, we designed a system to specifically induce carboxysome formation in vivo in *Synechococcus* PCC7942. Fluorescently tagged carboxysome components were used to monitor assembly using time-lapse microscopy. By tracking carboxysome formation with transmission electron microscopy, high-resolution images of assembly intermediates were captured. The architectural role of each gene product in the *ccm* operon was determined by systematically deleting each gene and monitoring the progression of carboxysome formation in the resulting mutant. Measurements of growth and photosynthetic activity confirmed the function of the carboxysomes generated by this system, providing additional validation criteria for constructing our model for assembly. The results of these studies enabled us to delineate the assembly pathway for the carboxysome and identify the specific *ccm* gene products required for progression through each stage of assembly.

RESULTS

A System to Investigate Dynamics of Carboxysome Biogenesis in *Synechococcus* PCC7942

An inducible system was designed to visually investigate carboxysome assembly in vivo, in order to study carboxysome biogenesis in the cyanobacterium *Synechococcus* PCC7942. First, we replaced the entire *ccm* operon with a Km^{R} cassette to generate the Δ*ccmK2-ccmO* (Δ*K2-O*) deletion strain (Figures 1B and S1 available online). Carboxysomes were not observed in the Δ*K2-O* strain using transmission electron microscopy (TEM); expression of RbcL-GFP or RbcL-CFP at a neutral site (NSII) with the P_{ccmK2} promoter in the Δ*K2-O* background that also

contained native RbcL resulted in diffuse fluorescence signal throughout the cell (Figures 1C and S1). Next, we generated an inducible *ccm* operon by replacing the native *ccm* promoter (P_{ccmK2}) with an isopropyl β-D-1-thiogalactopyranoside (IPTG)-inducible promoter (P_{trc}). The P_{trc}*::ccmK2-ccmO* operon was then introduced into the chromosome of the Δ*K2-O* mutant at a second neutral site (NSI) to generate the Δ*K2-O*$^+$ strain (Figure 1D).

To investigate the structural roles of each *ccm* gene product, we also generated inducible *ccm* operon variants systematically lacking each gene without drastically altering the upstream intergenic regions and targeted them to NSI (Figure 1D). Other fluorescently tagged carboxysome proteins were expressed from NSII in the Δ*K2-O*$^+$ strain to visually monitor the progression of carboxysome formation (Figure 1D).

Biogenesis of Functional Carboxysomes Can Be Tightly Controlled

Cyanobacterial strains lacking functional carboxysomes die in air but are able to survive in an atmosphere containing 3% CO_2. This high-CO_2 requiring phenotype (HCR) provided a robust screen for the correct assembly of carboxysomes; only strains with functional carboxysomes can survive in air. Using growth in air as a proxy for functional carboxysomes, we compared growth of the WT, Δ*K2-O*, Δ*K2-O*$^+$, and Δ*K2-O*$^+$/RbcL-GFP strains in air and 3% CO_2 in the presence and absence of 1 mM IPTG (Figure 2A). All strains grew similarly at 3% CO_2. The Δ*K2-O* strain was unable to grow in air, as expected. In contrast, the Δ*K2-O*$^+$ strains were only able to survive in air in the presence of IPTG (Figures 2A and S2). The dependence on IPTG for growth of the Δ*K2-O*$^+$ strains in air was apparent in liquid and solid medium (Figure S2). A threshold of 5 μM IPTG was required for growth in air, however, at this concentration cells appeared chlorotic and exhibited reduced growth (Figure S2C); an IPTG concentration of 0.2–1 mM was used for subsequent experiments. These results indicate that carboxysome biogenesis can be tightly controlled by modulating the expression of the *ccm* operon.

Photosynthetic Capacity of the Δ*K2-O*$^+$ Strain following Induction of the *ccm* Operon Is Equivalent to the WT

In photosynthetic organisms, CO_2 fixation is the major sink for the reducing equivalents and ATP derived from photochemistry (Krall and Edwards, 1992) (Figure 1A). Disruption of carbon fixation ultimately results in damage to photosystem II (PSII), the site of water oxidation (Takahashi and Murata, 2005). We estimated the relative photosynthetic capacity of PSII (Fv/Fm) by measuring chlorophyll fluorescence of dark-adapted cells grown in air and 3% CO_2 in the presence or absence of 1 mM IPTG (Figure 2B). The cells' ability to produce carboxysomes was positively correlated with Fv/Fm levels in air, and negatively correlated in 3% CO_2 (Figure 2B). The rapid drop in Fv/Fm levels of the Δ*K2-O*$^+$ strain and growth inhibition after transfer from 3% CO_2 to air (Figure 2C) was quickly restored following induction of the *ccm* operon (Figure 2D). These results indicate that the carboxysome directly influences the photosynthetic capacity of the cell by generating a sink for cellular reducing equivalents and

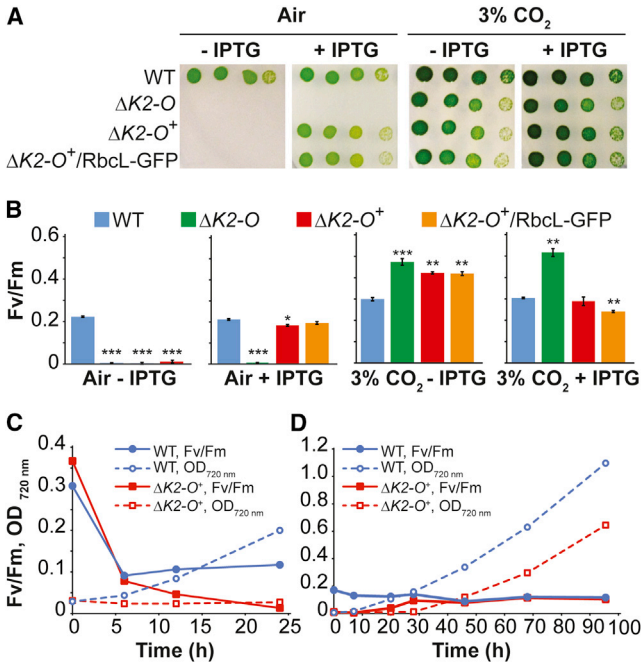

Figure 2. Physiology of Strains in Air and 3% CO_2

(A) Growth of strains in the presence and absence of IPTG. Ten-fold serial dilutions were plated and imaged after 72 hr.

(B) Photosynthetic capacity of photosystem II (Fv/Fm) after 24 hr growth in air or 3% CO_2. Data represent mean ± s.d. for three biological replicates; Means were compared to the WT (two-tailed Student's t test, n = 3). *p < 0.05, **p < 0.01, ***p < 0.001.

(C) Growth ($OD_{720\ nm}$) and Fv/Fm following transfer from 3% CO_2 to air without IPTG.

(D) Recovery of Δ*K2-O*$^+$ strain with 1 mM IPTG after 24 hr growth in air (C). See Figure S2 for additional data.

that upon induction of the *ccm* operon, the physiology of the Δ*K2-O*$^+$ strain is comparable to the WT.

Visualization of Carboxysome Biogenesis In Vivo by Time-Lapse Fluorescence Microscopy and TEM

Next, we investigated carboxysome biogenesis in Δ*K2-O*$^+$ strains constitutively expressing RbcL-GFP or RbcL-CFP following induction of the *ccm* operon using time-lapse fluorescence microscopy (Figure 3 and Movies S1 and S2). Upon induction of the *ccm* operon, the initially diffuse fluorescent signal rapidly (~30 min) coalesced into either a polar or midcell aggregate (Figure 3A and Movie S1). In rare instances two particles formed simultaneously; over time one was depleted at the expense of the other (i.e., the size of one particle increased as the size of the other particle decreased), ultimately leading to a single fluorescent punctum (Movie S1). A sedimentation assay was also used to monitor the aggregation of RuBisCO in the Δ*K2-O*$^+$ strain, which does not contain any fluorescently labeled protein. RuBisCO was initially retained in the soluble (S) fraction of cell-free lysates following centrifugation but the amount in the pellet (P) fraction increased as the time course progressed as determined biochemically by western blot using an α-RbcL antibody (Figure 3B). After ~2.5 hr postinduction, new particles emerged

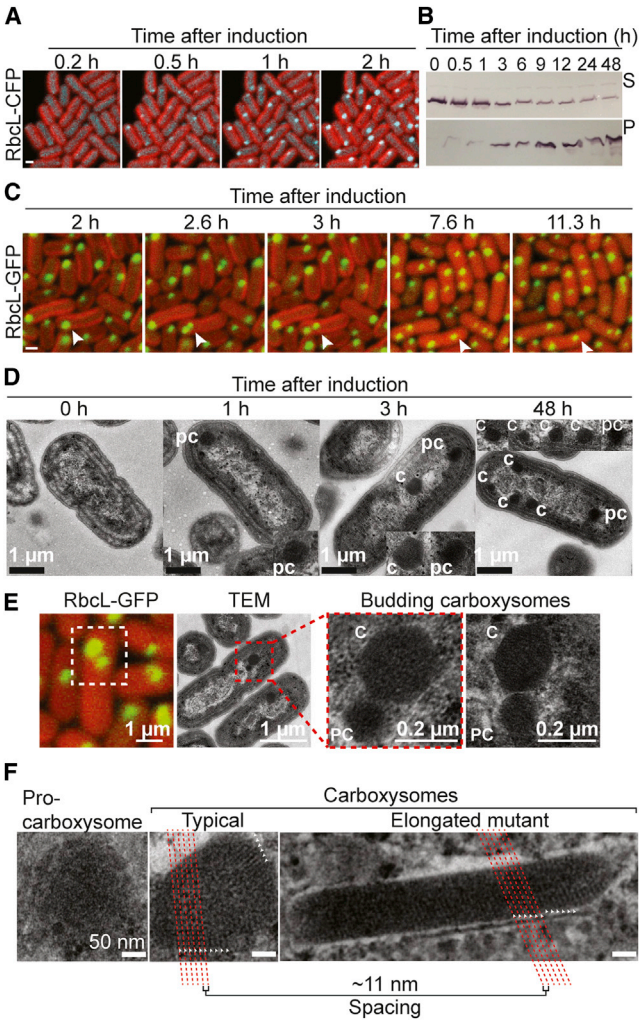

Figure 3. Visualization of Carboxysome Biogenesis

(A) Aggregation of RbcL-CFP (cyan) in Δ*K2-O*$^+$/RbcL-CFP/CcmK2-YFP strain following induction of *ccm* operon (Movie S1). Scale bars, 1 μm; Chl-*a*, red.

(B) Western blot showing soluble (S) and pelletable (P) fractions of Δ*K2-O*$^+$ lysate probed with α-RbcL.

(C) Progression of carboxysome formation in Δ*K2-O*$^+$ expressing RbcL-GFP (green) is marked with white arrows (Movie S2). Scale bars, 1 μm; Chl-*a*, red.

(D) TEM images of Δ*K2-O*$^+$ strain. Carboxysome, C; procarboxysome, PC.

(E) Budding carboxysomes in Δ*K2-O*$^+$/RbcL-GFP (green) strain (frame 55/200, Movie S2) and in Δ*K2-O*$^+$ strain with TEM. Two representative TEM images are shown.

(F) Procarboxysomes and carboxysomes can be morphologically distinguished. For additional data refer to Figure S3 and Movies S1 and S2.

from the polar RuBisCO aggregates (Figure 3C and Movies S2 and S2). Over the course of 10 hr (3 min interval between acquisitions) more than 100 individual budding events were observed (Figure S3). Moreover, following the rapid development of the primary particle, the number of new particles appeared to increase linearly over time, indicating that the newly formed particles are not dividing; this would be expected to result in an exponential increase in particle number (Figure S3). Once separated from the aggregate, the newly formed particle typically migrated to a more central position within the cell where it remained.

To further investigate the nature of the developing particle, TEM was used to follow induction of carboxysome formation in the Δ*K2-O*$^+$ strain (Figure 3D). The cells used for TEM were collected from the same culture used for western blot analysis (Figure 3B). Consistent with the fluorescence microscopy data, an electron dense polar body (Figure 3D) that we have designated as a procarboxysome (PC) appeared 1 hr postinduction. Polyhedral structures were first observed in the cell in addition to the PC after 3 hr. Multiple carboxysomes could be identified in the cell by the 48 hr time point. It is evident that the new particles emerging from the PC are carboxysomes based on their ultrastructure and the tight correlation between the induction of the *ccm* operon and the ability of the cells to survive in air. Budding carboxysomes were frequently observed in time-lapse movies and could also be identified in electron micrographs of cells harvested during induction of the carboxysome operon (Figure 3E). Two representative budding events are shown; typically a rounded, electron dense structure was observed adjacent to a polyhedral body. Carboxysomes and PCs could be morphologically distinguished in electron micrographs (Figures 3F and S3E). PCs were typically rounded electron dense structures with no discernible internal order; in contrast, carboxysomes typically exhibited a polyhedral profile and contained regularly spaced particles (Figure 3F). The spacing was particularly apparent in functional, disk-shaped carboxysomes that are frequently produced in a strain expressing CcmO-YFP. An average spacing of ~11 nm (Figure 3F) is consistent with that of packed L_8S_8 RuBisCO holoenzymes, in agreement with a previous study (Kaneko et al., 2006).

Elucidating the Hierarchy of Protein-Protein Interactions in Assembly of the Carboxysome

To determine the role of individual *ccm* gene products in the sequence of steps in carboxysome formation, inducible *ccm* operon variants lacking each gene (Δ*ccmK*, Δ*ccmL*, Δ*ccmM*, Δ*ccmN*, and Δ*ccmO*) were generated (Figure 4); the resulting strains were all HCR (Figures 4G–4L), in agreement with previous studies (Kinney et al., 2012; Ludwig et al., 2000; Marco et al., 1994; Price et al., 1993). Using RbcL-GFP as a visual marker, the phenotypes resulting from the expression of the *ccm* operon variants were analyzed 48 hr postinduction with 1 mM IPTG (Figures 4A–4F).

The Small Subunit-Like Domains of CcmM Are Required for Aggregation of RuBisCO and Initiation of Carboxysome Formation

Carboxysome formation was apparent in the control strain following induction (Δ*K2-O*$^+$/RbcL-GFP) (Figure 4A), conferring the ability to survive in air (Figure 4G). In contrast, RbcL-GFP remained soluble in the Δ*ccmM* mutant (Figure 4D). CcmM contains an N-terminal γ-carbonic anhydrase (γ-CA) (Peña et al., 2010) domain followed by three RbcS-like domains (Figure S4A). Two specific translation products, a full-length 58 kDa (M58) and a 35 kDa (M35) product, containing only the three RbcS-like domains, are crucial for carboxysome formation (Long et al., 2010). To further characterize the role of the RbcS-like domains,

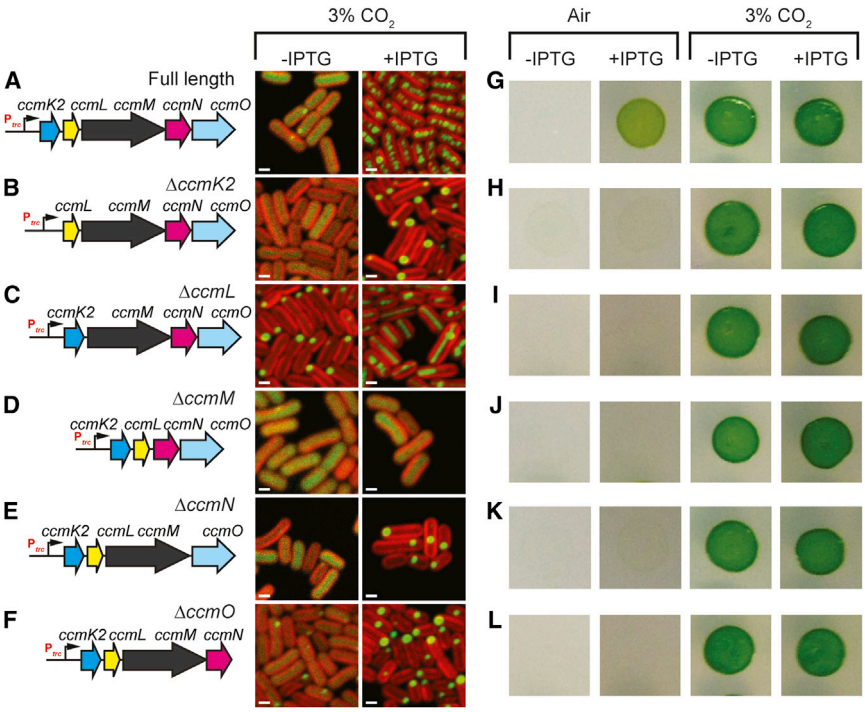

Figure 4. Role of *ccm* Gene Products during Carboxysome Biogenesis

(A–F) RbcL-GFP (green) was visualized before and after 48 hr induction of *ccm*-operon variants missing individual genes. Red channel is Chl-*a*. Scale bars, 1 μm.

(G–L) Growth of strains in air or 3% CO_2 in the presence or absence of 1 mM IPTG. Physiological data correspond to *ccm* operon variants (A)–(F) in the same row. Only the full-length *ccm* operon is able to confer growth in air upon addition of IPTG. All strains are able to survive in 3% CO_2. Also see Figure S4 for additional data related to the function of CcmM in carboxysome biogenesis.

we coexpressed them fused to YFP with RbcL-CFP in the Δ*K2-O* background (Figure S4B). Expression of M35-YFP or a truncated version (23 kDa; M23) containing two RbcS-like domains was sufficient to nucleate RbcL-CFP in the Δ*K2-O* mutant. In contrast, a single RbcS-like domain (11 kDa; M11) was not. Similarly, when GFP-tagged RbcS-like domains were expressed in WT cells, only the M35-GFP and M23-GFP appeared to exhibit carboxysome localization, while expression of M11-GFP resulted only in diffuse signal throughout the cell (Figure S4C). Expression of these constructs did not appear to alter the physiology of the parent strain; Δ*K2-O* strains expressing M35-YFP, M23-YFP, or M11-YFP fusion proteins exhibited HCR phenotypes and expression of the equivalent GFP-tagged fusion proteins in the WT strain did not affect its ability to survive in air. These results show that two or more RbcS-like domains of CcmM are required for initiation of carboxysome (PC) formation.

Shell Formation Is Dependent on the Association of CcmN with the PC, followed by the Concomitant Addition of CcmK2, and CcmO

The γ-CA domain of CcmM physically interacts with the N terminus of CcmN (Cot et al., 2008; Kinney et al., 2012). Thus, it is likely that CcmN associates with the PC upon aggregation of RuBisCO by CcmM. Carboxysome biogenesis stalls following PC formation in Δ*ccmN* strains, resulting in a single, polar RbcL-GFP aggregate (Figure 4E). In a fraction of the Δ*ccmN* cells (~8%, n = 1,110), a smaller fluorescent spot could be seen in addition to the PC; these were never observed in the Δ*ccmK2* (Figure 4B) or Δ*ccmO* (Figure 4F) strains. These foci could represent aborted PCs.

The phenotype of the Δ*ccmN* strain is comparable to that of the shell protein mutant strains Δ*ccmK2* (Figure 4B) and Δ*ccmO* (Figure 4F). The similarity in phenotype among these strains is notable because CcmN contains a C-terminal peptide (EP; encapsulation peptide) that interacts with CcmK2 and is essential for carboxysome formation; in strains lacking the encapsulation peptide only a polar aggregate is formed (Kinney et al., 2012). Therefore, we propose that CcmN recruits the shell protein CcmK2 to the PC. Consistent with this hypothesis, in the absence of CcmN, CcmK2 did not associate with the PC and carboxysomes were not produced (Figure 5A). Strikingly, in the Δ*ccmN* mutant, RbcL-CFP aggregated normally into the PC, while CcmK2-YFP began as a single, polar, fluorescent spot and ended up diffuse across the cell. Dispersal of the CcmK2-YFP focus was dependent on the presence of native (unlabeled) CcmK2, since this process did not occur in the Δ*ccmK2* strain; the fluorescence remained localized in a single spot. The propensity of CcmK2-YFP to remain fixed in an aggregate could explain why it alone is unable to rescue the HCR phenotype of Δ*ccmK2* strains. In addition to the requirement for CcmN (Figure 5B), localization of CcmK2 to the PC was dependent on the presence of CcmO (Figure 5C). Unlike CcmK2-YFP, CcmO-YFP exhibits a diffuse fluorescence signal throughout the cell prior to the induction of the *ccm* operon (Figure 5C). Upon induction of the full *ccm* operon, CcmO-YFP forms disk-like aggregates adjacent to the PC. However, CcmO-YFP remains soluble in the Δ*ccmK2* mutant and is unable to aggregate. CcmK2-YFP becomes soluble upon induction in the Δ*ccmO* strain, but carboxysomes are not formed. Together, these data demonstrate that shell formation around the PC requires CcmN first, and then the concomitant presence of CcmK2 and CcmO.

The Pentameric Vertex Protein, CcmL, Is Required for Budding of Carboxysomes from the PC

The carboxysome shell is capped by the pentameric vertex protein, CcmL (Figure 1A) (Tanaka et al., 2008). In the absence of CcmL, elongated structures developed from the PC in the majority of cells (~92%, n = 1371), while a few cells (~6%, n = 1371) appeared similar to WT (Figure 4C). PCs are observed prior to induction in the Δ*ccmL* strain. This is likely due to leaky expression

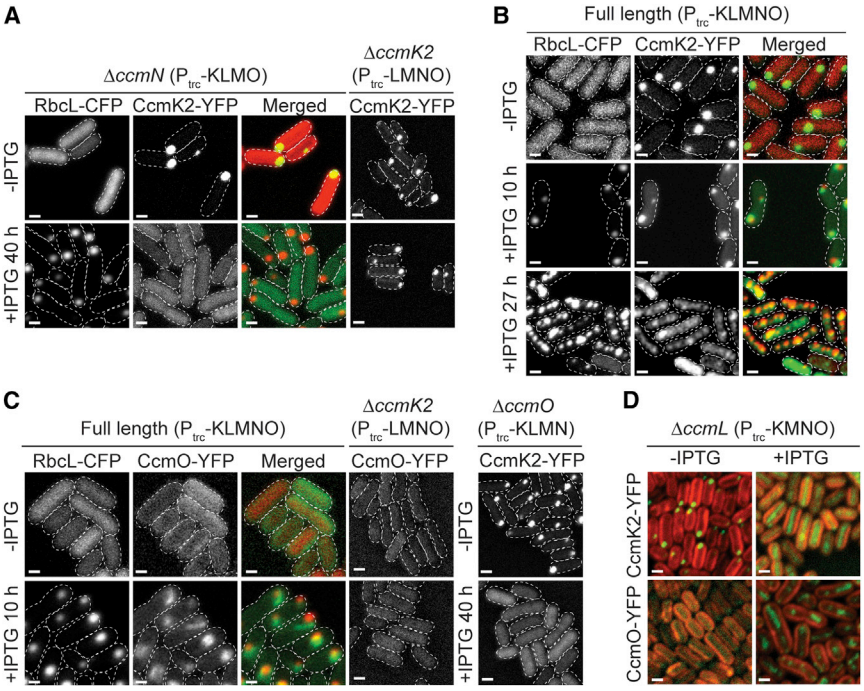

Figure 5. Interactions between Shell Proteins and Carboxysome Interior

(A) CcmN is required for recruitment of CcmK2 (green) to the PC. Solubilization of CcmK2-YFP depends on unlabeled CcmK2.

(B) CcmK2-YFP (green) associates with the PC and carboxysome.

(C) Shell formation requires simultaneous presence of CcmO (green) and CcmK2.

(D) Elongated carboxysomes in Δ*ccmL* are encapsulated by CcmK2 and CcmO.

Scale bars, 1 μm. The Chl-*a* channel was used as a template for cell outlines. RbcL-CFP, red (A, B, and C). Chl-*a*, red (D). See also Figures S1 and S5.

of *ccmM*, resulting from the disruption of the *ccm* operon just upstream of *ccmM*. Some leakage is also observed in the control strain prior to induction, but is not seen in the Δ*ccmM* mutant (Figure 4D). Rod-like carboxysomes are rare in WT cells expressing RbcL-GFP (~3%, n = 1,515), but were occasionally observed in Δ*K2-O*$^{+}$/RbcL-GFP or RbcL-CFP strains (Figure S5 and Movies S1 and S2). The elongated carboxysomes in the Δ*ccmL* mutant are encapsulated with a shell that contains CcmK2-YFP and CcmO-YFP (Figure 5D). Encapsulation appears to drive elongation by constricting the diameter of the PC, while incorporation of the pentamer promotes shell closure and subsequent budding.

A Model for Carboxysome Biogenesis in *Synechococcus* PCC7942

Together these data enabled us to generate a stepwise model for carboxysome biogenesis (Figure 6). First, soluble RuBisCO coalesces into a PC in a process dependent on CcmM, specifically the M35 translation product containing three RbcS-like domains. CcmN is added to the PC through interactions with N-terminal γ-CA domain of full-length CcmM (Cot et al., 2008; Kinney et al., 2012). The CcmN C-terminal encapsulation peptide (Kinney et al., 2012) on the surface of the PC interacts with assembling shell proteins; shell formation is dependent on the presence of both CcmK2 and CcmO. Upon incorporation of CcmL, fully encapsulated carboxysomes are released from the PC and migrate to a new cellular position, likely through interactions with the cytoskeleton (Savage et al., 2010).

Fate of Carboxysomes during Growth of Cyanobacteria

During stationary phase, *Synechococcus* PCC7942 cells elongate into extended filaments due to reduced cell division as a result of nutrient depletion (Goclaw-Binder et al., 2012). Microscopic examination of stationary phase cells grown in air and expressing RbcL-CFP (cyan) and M35-YFP (green) reveals that these highly elongated, filamentous cells contained numerous carboxysomes (Figures 7 and S6). Moreover, endogenous chlorophyll-*a* (red) fluorescence was only observed in cells containing carboxysomes. The rest of the cells exhibited no detectable chlorophyll-a signal and only contained soluble RbcL-CFP. The presence of chlorophyll suggests that the elongated cells containing carboxysomes are photosynthetically active and viable. Moreover, these results indicate that carboxysome stability could be an important factor in maintaining cellular fitness during extended periods of growth and during nutrient limitation.

DISCUSSION

The cyanobacterial carboxysome is a large (~300 MDa) self-assembling macromolecular bacterial organelle for CO_2 fixation. Understanding the assembly of functional carboxysomes has been hampered by experimental limitations in spatial and temporal resolution. High-resolution images of carboxysomes have been acquired using electron microscopy, however, these static images have not enabled researchers to confidently identify intermediates in the carboxysome biogenesis pathway (Iancu et al., 2010). During steady-state growth of cyanobacteria, it is likely that only a subset of the cells are assembling carboxysomes at any one instant. Moreover, one rarely observes intermediates in an embedded thin section because the majority of carboxysomes are not undergoing biogenesis. Our system utilizes an inducible system to turn on carboxysome biogenesis simultaneously in an entire culture (Figure 1). This synchronization has enabled us to identify each step of carboxysome biogenesis using high-resolution electron microscopy and visualize the process in real-time using fluorescence microscopy (Figure 3 and Movies S1 and S2).

While heterologous expression and characterization of carboxysomes and other BMCs in *E. coli* has provided insight into the components necessary for assembly (Bonacci et al., 2012; Choudhary et al., 2012; Parsons et al., 2008), using the native

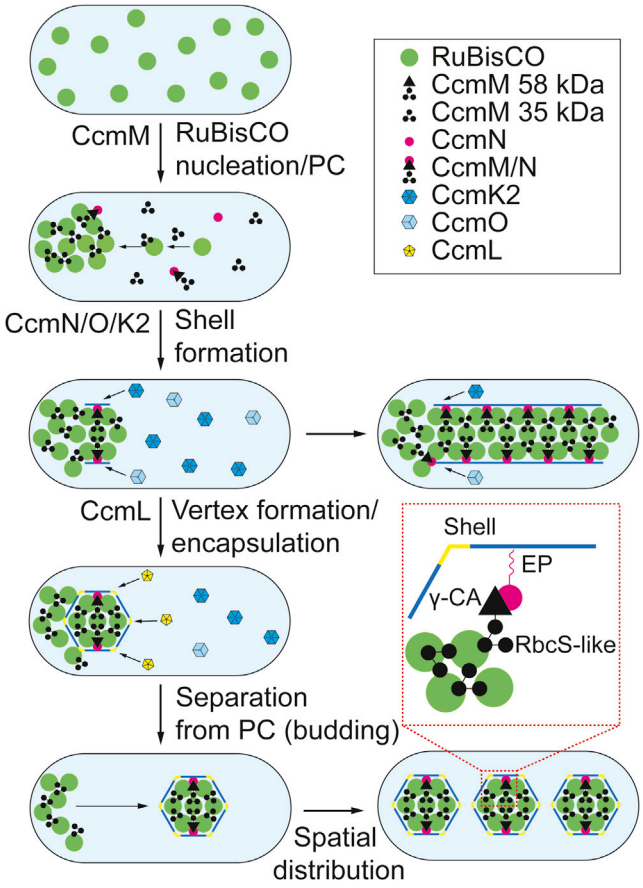

Figure 6. Model of Carboxysome Biogenesis in *Synechococcus* PCC7942

Prior to carboxysome formation, RuBisCO exists as a soluble protein. Full-length (M58) and short (M35) forms of CcmM aggregate RuBisCO into the procarboxysome (PC). CcmN is brought to the PC through interactions with CcmM, where the C-terminal encapsulation peptide (EP) recruits shell proteins, ultimately leading the encapsulation by CcmK2 and CcmO. Encapsulation of the PC and release of functional carboxyomes requires the incorporation of the pentameric vertex protein, CcmL. Once fully encapsulated, the interior of the carboxysome no longer interacts with the PC and the fully formed carboxysome separates from the PC. This process is repeated until the PC has been depleted.

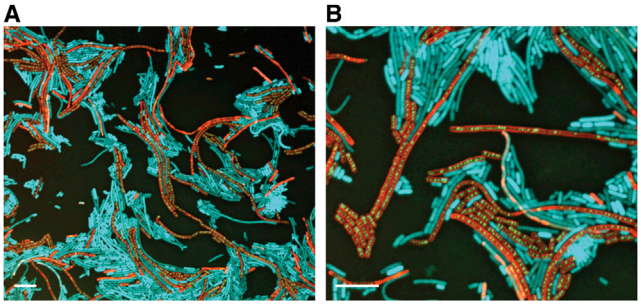

Figure 7. Persistence of Carboxysomes in Stationary Phase Cells

(A and B) Elongated cells typically found in stationary phase *Synechococcus* 7942 cells contain carboxysomes. The cells pictured were grown on solid BG11 media in air for approximately 30 days. Only cells containing carboxysomes also exhibit Chl-*a* fluorescence (red) indicating that these cells are photosynthetically active and viable. RbcL-CFP (cyan) is diffuse in cells lacking carboxysomes. "CcmM" M35-YFP (green) was used as a marker to track carboxysomes. Scale bars, 10 μm. Individual channels used to create these composite images are shown in Figure S6.

host provided us a strong selection for the generation of functional carboxysomes, since they are essential in cyanobacteria for growth in air (Figures 2 and S2). In addition, we were able to measure the effects of enzyme encapsulation on the physiology of the host strain (Figures 2B and 2C). We found that the photosynthetic capacity of the cell was directly related to the presence or absence of carboxysomes (Figures 2B and 2C). As expected, we found that carboxysomes are required for photosynthesis and growth in air, but we also found that they likely play a role in survival during stationary phase (Figure 7). The increased Fv/Fm observed in carboxysome-less cells grown in 3% CO_2 is likely due to increased levels of photorespiration catalyzed by free RuBisCO. In fact, this strain provides an ideal background to study cellular physiology during carbon fixation in cyanobacteria by directly modulating the carbon fixing apparatus in vivo.

Prior to this study, it was known that each gene in the *ccm* operon is essential for growth in air and for carboxysome formation (Kinney et al., 2012; Ludwig et al., 2000; Marco et al., 1994; Price et al., 1993). However, the specific role for each of the components was based on a static view provided by genetic and microscopic analysis. Our experimental system enabled us to combine techniques with high spatial (TEM) and temporal (fluoresecence microscopy and physiological measurements) resolution to systematically investigate the role played by each product of the *ccm* operon during carboxysome assembly (Figures 4 and 6).

Carboxysome biogenesis in *Synechococcus* PCC7942 is initiated upon aggregation of RuBisCO in a process that is dependent on CcmM (Figure 4D), specifically the RbcS-like domains (Figure S4). During this process, RuBisCO rapidly coalesces into a discrete punctum, typically at a cellular pole (Figure 3). The resulting PC contains disordered RuBisCO particles (Figure 3F) that are not yet encapsulated. These results clearly demonstrate that the interior components of the carboxysome assemble first, prior to encapsulation, in contrast to speculation based on TEM images that the shell is formed first and then packed with RuBisCO (Price and Badger, 1991). Moreover, our results are consistent with models in which RuBisCO appears to be simultaneously aggregated and encapsulated, leading to the presence of partially formed carboxysomes (Iancu et al., 2010). However, the carboxysomes studied by Iancu et al. (from chemoautotrophic bacteria) do not contain CcmM and the mechanism for RuBisCO aggregation in these types of carboxysomes is unknown. Stalled products of carboxysome formation could be the result of insufficient amounts of RuBisCO or shell proteins.

In addition to a role in formation of the PC, CcmM has been shown to physically interact with CcaA (Cot et al., 2008) and CcmN (Kinney et al., 2012), providing a means for these proteins to associate with the procarboxysome. CcmN contains an encapsulation peptide that has been shown to interact with

the major shell protein CcmK2 (Kinney et al., 2012). We found that CcmN is required for shell proteins to associate with the PC (Figures 4 and 5). Our results also indicate that assembly of shells on the PC drives the budding of new carboxysomes. In the absence of CcmN, only PCs form and budding is not observed. Assembly of the carboxysome shell is also dependent on the simultaneous presence of both CcmK2 and CcmO (Figure 5). In fact, soluble CcmO-YFP was able to assemble into disks adjacent to the PC only if CcmK2 was present. Interactions between CcmK2 and CcmO have been previously observed (Rae et al., 2012), however, the molecular arrangement of specific proteins within the carboxysome shell is thus far unknown. Moreover, genes encoding the shell proteins *ccmK3*, *ccmK4*, and *ccmP* are present in the Δ*K2-O* background. While not essential for carboxysome formation, these shell proteins could play an important role in defining the biochemical properties of the shell (Cai et al., 2013; Rae et al., 2012).

The pentameric vertex protein CcmL is essential for carboxysome function because removal of the *ccmL* gene from the *ccm* operon resulted in a HCR phenotype (Figures 4C and 4I) as previously described for a *ccmL* insertion mutant (Price and Badger, 1989). In the absence of CcmL, rod-like carboxysomes encapsulated by CcmK2 and CcmO (Figure 5D) are formed in the majority of cells, often protruding from the PC (Figures 4C, 5D, S5, and 6). Our results indicate that the protrusion of the elongated carboxysome from the PC is driven by shell formation while incorporation of the pentamer allows closure of the compartment and subsequent budding from the PC. Some Δ*ccmL* cells also contain apparently normal looking carboxysomes (Figures 4C and 4I). We suspect they are nonfunctional since the Δ*ccmL* strain is unable to survive in air. Occasionally, we observed Δ*ccmL* cells without any fluorescent signal. This may be the result of asymmetric distribution of the elongated structure following cell division. In fact, the elongated carboxysomes were often seen in the midcell constriction, preventing cell division (Figure S5A). Previous work found that pentameric vertex proteins are required to prevent leakage of CO_2 from carboxysomes in *Halothiobacillus neapolitanus* (Cai et al., 2009). However, in the deletion strains lacking both the of the vertex proteins of the *H. neapolitanus* carboxysome, only a small fraction of the cells contained elongated carboxysomes. The reduced number of elongated carboxysomes in this strain compared to the Δ*ccmL* presented here may be due to differences in the level of RuBisCO available for carboxysome biogenesis in a deletion mutant during steady-state growth compared to our inducible system with the capacity to generate multiple carboxysomes de novo.

Our model for carboxysome biogenesis provides a specific role for each gene product of the *ccm* operon. Since assembly pathways for protein complexes are under strong evolutionary selection (Marsh et al., 2013), and because BMCs are defined by a common shell architecture, we propose that the principles that we have deduced for carboxysome assembly apply to diverse BMCs. For example, disruption of the Pdu metabolosome shell protein, PduA, in *Salmonella enterica* results in a large polar body that contains the major enzyme of the compartment interior, diol dehydratase, and is reminiscent of the procarboxysome (Havemann et al., 2002). In BMCs that apparently lack an interior scaffolding protein like CcmM, organization of the interior could be accomplished through the oligomerization of multimeric enzymes prior to encapsulation (Bovell and Warncke, 2013) followed by interactions between the shell and interior components facilitated by encapsulation peptides (Fan et al., 2012; Kinney et al., 2012). Accordingly, understanding the assembly pathway of the carboxysome provides the conceptual framework for investigating the biogenesis of medically and biotechnologically important BMCs and for constructing novel bacterial organelles for bioengineering applications.

In summary, this is the first description of the biogenesis of a bacterial organelle in vivo. In contrast to eukaryotic organelles to which cargo is targeted across the bounding membrane, in the hierarchy of steps in carboxysome assembly, those for form follow those for function: the carboxysome assembles its contents into a procarboxysome first; encapsulation in the delimiting protein shell is the penultimate step before budding and cellular localization.

EXPERIMENTAL PROCEDURES

Strains and Plasmids

Wild-type *Synechococcus elongatus* PCC7942 was used as the background strain for all genetic manipulation. All strains used in this study are listed in Table S1. Oligonucleotides used in cloning and segregation analysis are listed in Table S2. Additional details about the generation of strains can be found in Extended Experimental Procedures. Standard molecular biology procedures were used for the construction of plasmids. In brief, a BglBrick strategy (Anderson et al., 2010) was used for the fusion of genes, fluorescent tags, and promoters and for the introduction of gene constructs into transformation vectors for integration into the chromosome specific loci, neutral site I and II, as described in Extended Experimental Procedures. Genetic deletions were generated via homologous recombination as previously described (Clerico et al., 2007).

Growth and Physiology

Strains were grown in BG11 (Allen, 1968) media in a Sanyo Environmental Chamber with an atmosphere containing air or 3% CO_2 and a light intensity of 100 μmol photons m^{-2} s^{-1}. Chlorophyll fluorescence kinetics were measured on an AquaPen-C fluorometer (Photon Systems Instruments, Brno, Czech Republic) using cells diluted to a Chl-*a* concentration of ~1–2 μg/ml and dark-adapted for 3 min.

Protein Extraction and Western Blotting

Cells harvested following induction with 200 μM IPTG were ruptured with glass beads. Soluble and pelletable fractions were collected from cell-free lysates following centrifugation as described in Extended Experimental Procedures. Proteins were separated by SDS-PAGE, transferred to nitrocellulose membranes, probed with rabbit α-RbcL (1:5,000; Agrisera) followed by goat α-rabbit IgG (1:7,500; Promega), and developed with SIGMAFAST BCIP/NBT (Sigma).

Microscopy

Fluorescence microscopy was performed on a Zeiss LSM 710 confocal microscope with a 63x/1.4 NA oil-immersion objective using cells plated on 1% agarose as described in Extended Experimental Procedures. Images were analyzed with ImageJ (Abramoff et al., 2004). For transmission electron microscopy, cells fixed with 2% glutaraldehyde were stained and embedded as described in Extended Experimental Procedures and imaged with a JEOL 1200 EX TEM (80 kV) or a FEI Technai 12 TEM (120 kV).

SUPPLEMENTAL INFORMATION

Supplemental Information includes Extended Experimental Procedures, six figures, two tables, and two movies and can be found with this article online at http://dx.doi.org/10.1016/j.cell.2013.10.044.

AUTHOR CONTRIBUTIONS

J.C.C. and C.A.K. designed the experiments. J.C.C. and S.C.W. constructed the strains and plasmids and performed the western blot. J.C.C. performed the fluorescence microscopy and physiological characterizations. J.C.C. and S.L.B. performed the electron microscopy. J.C.C and C.A.K. wrote the manuscript. All authors approved the final manuscript.

ACKNOWLEDGMENTS

We thank members of the Kerfeld laboratory for helpful discussions. We thank Dr. Gustaf Sandh for construction of the Δ*K2-O* deletion plasmid and Patrick Shih for generating BglBrick modified neutral site vectors. We thank Dr. Kent McDonald, Reena Zalpuri, and Desiree Stanley for assistance with electron microscopy. We thank Dr. Susan Golden for providing pAM2314, pAM1573, and pAM2991 vectors and Dr. David Savage for providing pDFS648. Funding for this work was provided by the NSF Emerging Frontiers Program (EF1105897).

Received: June 8, 2013
Revised: July 30, 2013
Accepted: October 25, 2013
Published: November 21, 2013

REFERENCES

Abramoff, M.D., Magalhaes, P.J., and Ram, S.J. (2004). Image processing with ImageJ. Biophotonics international *11*, 36–42.

Allen, M.M. (1968). Simple conditions for growth of unicellular blue-green algae on plates. J. Phycol. *4*, 1–4.

Anderson, J.C., Dueber, J.E., Leguia, M., Wu, G.C., Goler, J.A., Arkin, A.P., and Keasling, J.D. (2010). BglBricks: A flexible standard for biological part assembly. J Biol Eng *4*, 1.

Bobik, T.A. (2006). Polyhedral organelles compartmenting bacterial metabolic processes. Appl. Microbiol. Biotechnol. *70*, 517–525.

Bobik, T.A., Havemann, G.D., Busch, R.J., Williams, D.S., and Aldrich, H.C. (1999). The propanediol utilization (*pdu*) operon of *Salmonella enterica* serovar Typhimurium LT2 includes genes necessary for formation of polyhedral organelles involved in coenzyme $B_{(12)}$-dependent 1, 2-propanediol degradation. J. Bacteriol. *181*, 5967–5975.

Bonacci, W., Teng, P.K., Afonso, B., Niederholtmeyer, H., Grob, P., Silver, P.A., and Savage, D.F. (2012). Modularity of a carbon-fixing protein organelle. Proc. Natl. Acad. Sci. USA *109*, 478–483.

Bovell, A.M., and Warncke, K. (2013). The structural model of Salmonella typhimurium ethanolamine ammonia-lyase directs a rational approach to the assembly of the functional $[(EutB\text{-}EutC)_2]_3$ oligomer from isolated subunits. Biochemistry *52*, 1419–1428.

Brinsmade, S.R., Paldon, T., and Escalante-Semerena, J.C. (2005). Minimal functions and physiological conditions required for growth of *salmonella enterica* on ethanolamine in the absence of the metabolosome. J. Bacteriol. *187*, 8039–8046.

Cai, F., Menon, B.B., Cannon, G.C., Curry, K.J., Shively, J.M., and Heinhorst, S. (2009). The pentameric vertex proteins are necessary for the icosahedral carboxysome shell to function as a CO_2 leakage barrier. PLoS ONE *4*, e7521.

Cai, F., Sutter, M., Cameron, J.C., Stanley, D.N., Kinney, J.N., and Kerfeld, C.A. (2013). The structure of CcmP, a tandem bacterial microcompartment domain protein from the β-carboxysome, forms a subcompartment within a microcompartment. J. Biol. Chem. *288*, 16055–16063.

Cannon, G.C., English, R.S., and Shively, J.M. (1991). In situ assay of ribulose-1,5-bisphosphate carboxylase/oxygenase in *Thiobacillus neapolitanus*. J. Bacteriol. *173*, 1565–1568.

Cannon, G.C., Bradburne, C.E., Aldrich, H.C., Baker, S.H., Heinhorst, S., and Shively, J.M. (2001). Microcompartments in prokaryotes: carboxysomes and related polyhedra. Appl. Environ. Microbiol. *67*, 5351–5361.

Cheng, S., Liu, Y., Crowley, C.S., Yeates, T.O., and Bobik, T.A. (2008). Bacterial microcompartments: their properties and paradoxes. Bioessays *30*, 1084–1095.

Choudhary, S., Quin, M.B., Sanders, M.A., Johnson, E.T., and Schmidt-Dannert, C. (2012). Engineered protein nano-compartments for targeted enzyme localization. PLoS ONE *7*, e33342.

Clerico, E.M., Ditty, J.L., and Golden, S.S. (2007). Specialized techniques for site-directed mutagenesis in cyanobacteria. Methods Mol. Biol. *362*, 155–171.

Cot, S.S., So, A.K., and Espie, G.S. (2008). A multiprotein bicarbonate dehydration complex essential to carboxysome function in cyanobacteria. J. Bacteriol. *190*, 936–945.

Fan, C., Cheng, S., Sinha, S., and Bobik, T.A. (2012). Interactions between the termini of lumen enzymes and shell proteins mediate enzyme encapsulation into bacterial microcompartments. Proc. Natl. Acad. Sci. USA *109*, 14995–15000.

Goclaw-Binder, H., Sendersky, E., Shimoni, E., Kiss, V., Reich, Z., Perelman, A., and Schwarz, R. (2012). Nutrient-associated elongation and asymmetric division of the cyanobacterium *Synechococcus* PCC 7942. Environ. Microbiol. *14*, 680–690.

Havemann, G.D., Sampson, E.M., and Bobik, T.A. (2002). PduA is a shell protein of polyhedral organelles involved in coenzyme B(12)-dependent degradation of 1,2-propanediol in Salmonella enterica serovar typhimurium LT2. J. Bacteriol. *184*, 1253–1261.

Iancu, C.V., Morris, D.M., Dou, Z., Heinhorst, S., Cannon, G.C., and Jensen, G.J. (2010). Organization, structure, and assembly of α-carboxysomes determined by electron cryotomography of intact cells. J. Mol. Biol. *396*, 105–117.

Kaneko, Y., Danev, R., Nagayama, K., and Nakamoto, H. (2006). Intact carboxysomes in a cyanobacterial cell visualized by hilbert differential contrast transmission electron microscopy. J. Bacteriol. *188*, 805–808.

Kerfeld, C.A., Sawaya, M.R., Tanaka, S., Nguyen, C.V., Phillips, M., Beeby, M., and Yeates, T.O. (2005). Protein structures forming the shell of primitive bacterial organelles. Science *309*, 936–938.

Kerfeld, C.A., Heinhorst, S., and Cannon, G.C. (2010). Bacterial microcompartments. Annu. Rev. Microbiol. *64*, 391–408.

Kinney, J.N., Salmeen, A., Cai, F., and Kerfeld, C.A. (2012). Elucidating essential role of conserved carboxysomal protein CcmN reveals common feature of bacterial microcompartment assembly. J. Biol. Chem. *287*, 17729–17736.

Kofoid, E., Rappleye, C., Stojiljkovic, I., and Roth, J. (1999). The 17-gene ethanolamine (*eut*) operon of *Salmonella typhimurium* encodes five homologues of carboxysome shell proteins. J. Bacteriol. *181*, 5317–5329.

Krall, J.P., and Edwards, G.E. (1992). Relationship between photosystem II activity and CO_2 fixation in leaves. Physiol. Plant. *86*, 180–187.

Long, B.M., Badger, M.R., Whitney, S.M., and Price, G.D. (2007). Analysis of carboxysomes from *Synechococcus* PCC7942 reveals multiple Rubisco complexes with carboxysomal proteins CcmM and CcaA. J. Biol. Chem. *282*, 29323–29335.

Long, B.M., Tucker, L., Badger, M.R., and Price, G.D. (2010). Functional cyanobacterial β-carboxysomes have an absolute requirement for both long and short forms of the CcmM protein. Plant Physiol. *153*, 285–293.

Ludwig, M., Sultemeyer, D., and Price, G.D. (2000). Isolation of *ccmKLMN* Genes From the Marine Cyanobacterium, *Synechococcus* sp. PCC7002 (Cyanophyceae), and Evidence that CcmM is Essential for Carboxysome Assembly. J. Phycol. *36*, 1109–1118.

Marco, E., Martinez, I., Ronen-Tarazi, M., Orus, M.I., and Kaplan, A. (1994). Inactivation of *ccmO* in *Synechococcus* sp. Strain PCC 7942 Results in a Mutant Requiring High Levels of $CO_{(2)}$. Appl. Environ. Microbiol. *60*, 1018–1020.

Marcus, Y., Berry, J.A., and Pierce, J. (1992). Photosynthesis and photorespiration in a mutant of the cyanobacterium *Synechocystis* PCC 6803 lacking carboxysomes. Planta *187*, 511–516.

Marsh, J.A., Hernández, H., Hall, Z., Ahnert, S.E., Perica, T., Robinson, C.V., and Teichmann, S.A. (2013). Protein complexes are under evolutionary selection to assemble via ordered pathways. Cell *153*, 461–470.

Orus, M.I., Rodriguez, M.L., Martinez, F., and Marco, E. (1995). Biogenesis and Ultrastructure of Carboxysomes from Wild Type and Mutants of *Synechococcus* sp. Strain PCC 7942. Plant Physiol. *107*, 1159–1166.

Parsons, J.B., Dinesh, S.D., Deery, E., Leech, H.K., Brindley, A.A., Heldt, D., Frank, S., Smales, C.M., Lünsdorf, H., Rambach, A., et al. (2008). Biochemical and structural insights into bacterial organelle form and biogenesis. J. Biol. Chem. *283*, 14366–14375.

Peña, K.L., Castel, S.E., de Araujo, C., Espie, G.S., and Kimber, M.S. (2010). Structural basis of the oxidative activation of the carboxysomal γ-carbonic anhydrase, CcmM. Proc. Natl. Acad. Sci. USA *107*, 2455–2460.

Price, G.D., and Badger, M.R. (1989). Isolation and Characterization of High $CO_{(2)}$-Requiring-Mutants of the Cyanobacterium *Synechococcus* PCC7942 : Two Phenotypes that Accumulate Inorganic Carbon but Are Apparently Unable to Generate $CO_{(2)}$ within the Carboxysome. Plant Physiol. *91*, 514–525.

Price, G.D., and Badger, M.R. (1991). Evidence for the role of carboxysomes in the cyanobacterial CO_2-concentrating mechanism. Can. J. Bot. *69*, 963–973.

Price, G.D., Coleman, J.R., and Badger, M.R. (1992). Association of Carbonic Anhydrase Activity with Carboxysomes Isolated from the Cyanobacterium *Synechococcus* PCC7942. Plant Physiol. *100*, 784–793.

Price, G.D., Howitt, S.M., Harrison, K., and Badger, M.R. (1993). Analysis of a genomic DNA region from the cyanobacterium *Synechococcus* sp. strain PCC7942 involved in carboxysome assembly and function. J. Bacteriol. *175*, 2871–2879.

Price, G.D., Badger, M.R., Woodger, F.J., and Long, B.M. (2008). Advances in understanding the cyanobacterial CO_2-concentrating-mechanism (CCM): functional components, Ci transporters, diversity, genetic regulation and prospects for engineering into plants. J. Exp. Bot. *59*, 1441–1461.

Rae, B.D., Long, B.M., Badger, M.R., and Price, G.D. (2012). Structural determinants of the outer shell of β-carboxysomes in *Synechococcus elongatus* PCC 7942: roles for CcmK2, K3-K4, CcmO, and CcmL. PLoS ONE *7*, e43871.

Savage, D.F., Afonso, B., Chen, A.H., and Silver, P.A. (2010). Spatially ordered dynamics of the bacterial carbon fixation machinery. Science *327*, 1258–1261.

Shively, J.M., Ball, F., Brown, D.H., and Saunders, R.E. (1973). Functional organelles in prokaryotes: polyhedral inclusions (carboxysomes) of *Thiobacillus neapolitanus*. Science *182*, 584–586.

So, A.K., John-McKay, M., and Espie, G.S. (2002). Characterization of a mutant lacking carboxysomal carbonic anhydrase from the cyanobacterium *Synechocystis* PCC6803. Planta *214*, 456–467.

Stojiljkovic, I., Bäumler, A.J., and Heffron, F. (1995). Ethanolamine utilization in *Salmonella typhimurium*: nucleotide sequence, protein expression, and mutational analysis of the *cchA cchB eutE eutJ eutG eutH* gene cluster. J. Bacteriol. *177*, 1357–1366.

Takahashi, S., and Murata, N. (2005). Interruption of the Calvin cycle inhibits the repair of Photosystem II from photodamage. Biochim. Biophys. Acta *1708*, 352–361.

Tanaka, S., Kerfeld, C.A., Sawaya, M.R., Cai, F., Heinhorst, S., Cannon, G.C., and Yeates, T.O. (2008). Atomic-level models of the bacterial carboxysome shell. Science *319*, 1083–1086.

Yeates, T.O., Kerfeld, C.A., Heinhorst, S., Cannon, G.C., and Shively, J.M. (2008). Protein-based organelles in bacteria: carboxysomes and related microcompartments. Nat. Rev. Microbiol. *6*, 681–691.